J Solid State Electrochem (2002) 6: 302–310
DOI 10.1007/s100080100237

ORIGINAL PAPER

**Eimutis Juzeliūnas · Konstantinas Leinartas
Meilutė Samulevičienė · Aloyzas Sudavičius
Povilas Miečinskas · Remigijus Juškėnas
Vaclovas Lisauskas**

Microgravimetric corrosion study of magnetron-sputtered Co-Cr-Mo and Ni-Cr-Mo alloys in an oxygen-containing atmosphere

Received: 6 March 2001 / Accepted: 10 July 2001 / Published online: 8 September 2001

Abstract A quartz crystal microbalance (QCM) has been used for in situ corrosion studies of magnetron-sputtered Co-Cr-Mo and Ni-Cr-Mo alloys, which are of great importance in various technical and medical applications. The corrosion monitoring has been performed in an oxygen-containing atmosphere and in NaCl solution. The alloys were deposited on quartz substrates by means of DC magnetron sputtering. X-ray photoelectron spectroscopy analysis showed that the composition of the deposits was similar to that of the magnetron-sputtering targets. X-ray diffraction revealed an amorphous structure of the sputtered deposits, while the casting alloys had a crystalline structure. The polarization resistance of sputtered alloys in NaCl solution was higher than the activity of conventional alloys, which implied a superior corrosion resistance of the sputtered deposits. Corrosion was initiated by supplying oxygen gas into a wet argon atmosphere and the QCM detected corrosion with nanogram resolution as the increase in mass. Corrosion currents were calculated from the mass versus time curves. The QCM appeared to be an effective tool for corrosive characterization of sputtered alloys in gaseous environments. A corrosion current calculation in solution was complicated by metal transfer to the liquid phase.

Keywords Metallic biomaterials · Alloy corrosion · Magnetron sputtering · Microgravimetry · Quartz crystal microbalance

Introduction

Sputter deposition of alloys has attracted considerable attention in recent years as an effective tool to deposit corrosion-resistant coatings [1, 2, 3, 4, 5, 6, 7, 8, 9, 10, 11, 12, 13, 14, 15, 16]. The excellent anticorrosive stability was attributed mainly to chemical homogeneity and the amorphous properties of sputtered alloys, which are free from crystallographic defects such as dislocations, crystal imperfections, distortions, grain boundaries, second phase elements, etc. Because of this, the passive films formed spontaneously on amorphous alloys are more uniform and contain less weak sites when compared to films on crystalline surfaces. Hashimoto et al. [14, 18] studied amorphous Fe-Cr-P-C and Ni-Ta-P alloys and came to the conclusion that crystallization effects lead to deterioration of the corrosion resistance. However, precipitation of nanocrystallites with dimensions less than 20 nm could increase the corrosion resistance, as has been demonstrated by heat treatment of amorphous Zr-Cr and Al-Cr alloys [2, 3].

In order to evaluate the corrosion resistance of sputtered alloys, electrochemical methods are usually employed. The selection and application of electrochemical criteria for corrosion testing is often quite complicated. Some limitations of corrosion resistance evaluation by means of voltammetry and impedance spectroscopy have been highlighted previously when studying magnetron-sputtered metallic biomaterials [15, 16]. It has been shown that the impedance spectra did not exhibit, in low-frequency domain, a clear resistive behaviour from which the corrosion current density could be derived [16]. Moreover, the alloys often failed to exhibit clear Tafel regions, from which the corrosion current could be obtained by extrapolation procedures. The commonly used determination of breakdown potentials does not provide any direct information about the corrosion under real conditions, i.e. under open circuit conditions. It should also be noted that the electrochemical methods relate to measurements in solution, where conditions could be quite different from those in the atmosphere.

An advantage of corrosion investigations of sputtered coatings is the use of the quartz crystal microbalance

E. Juzeliūnas (✉) · K. Leinartas · M. Samulevičienė
A. Sudavičius · P. Miečinskas · R. Juškėnas · V. Lisauskas
Institute of Chemistry, A. Goštauto 9,
2600 Vilnius, Lithuania
E-mail: ejuzel@ktl.mii.lt

(QCM), which is a commonly known sensitive mass detector in both gaseous and liquid environments. It is important that the QCM is capable of supplying continuous information about the corrosion dynamics at any time, which is virtually impossible using conventional corrosion testing methods.

The QCM technique has been used for corrosion studies of many single metals, for instance Co [19], Ni [19, 20], Sn [20], Al [21], Cu [22, 23, 24, 25], Ag [24], Fe [26], Cd [27, 28] and Zn [29]. However, there is little work on QCM applications to multicomponent alloys. The main difficulty is the coating of quartz with an alloy layer of desirable composition and structural properties. The magnetron sputtering technique seems to be an effective alternative to conventional thermal evaporation or electroplating, as has been demonstrated by depositing Au-Pd-In [15, 16], Fe-Cr-Ni and Fe-Cr-Ni-Ta [17] as well as Fe-Cr-Mo [12] on quartz for QCM measurements.

This work aims to study, using QCM, the corrosion of magnetron-sputtered Co-Cr-Mo and Ni-Cr-Mo alloys. While the main attention has been focused on performing investigations in an oxygen-containing atmosphere, some experiments in NaCl solution were carried out as well. Efforts have been made to demonstrate that the QCM represents a promising approach for in situ corrosion monitoring of highly resistant magnetron-sputtered alloys in gaseous environments.

Experimental

Targets for magnetron sputtering (MS) were prepared from commercially available alloys by melting them into discs with radius 25 mm (exact compositions of the targets are given in Tables 1 and 2). The Co-Cr-Mo specimen was a Remanium GM380 dental alloy as received from Dentaurum (Germany) and the Ni-Cr-Mo alloy was a Ney Quantom alloy produced by Ney Dental International (USA). The vacuum in the MS chamber was maintained at 1.33×10^{-4} Pa. The working gas was argon and its pressure was maintained at 0.1–0.2 Pa. The temperature in the chamber was ca. 100 °C. The argon ionization current was 60 mA and the voltage was 600 V. The sputtering duration was 12–15 min, which corresponded to a coating thickness of ca. 0.15–0.2 μm. More details about the MS procedure used are given elsewhere [15, 16, 17].

To minimize oxide formation during Co-Cr-Mo and Ni-Cr-Mo sputtering, the target was pre-cleaned mechanically with abrasive paper. With the same aim, the chamber was treated at 200 °C for 20 h. Pure argon (99.999%; Messer Griesheim) was used as the working gas.

The substrates for MS were quartz discs, 15 mm in diameter (AT plane), produced by KVG Quartz Crystal Technology (Germany). One side of the crystal was coated by gold and the other side was coated by an alloy of interest using the MS technique. Prior to magnetron sputter deposition, the quartz surfaces were cleaned ultrasonically in pure acetone (99.999%). Four quartz discs were mounted in a special holder for simultaneous plating in the MS chamber. The differences in chemical composition on different quartz discs were negligible.

The coating composition was analysed by X-ray photoelectron spectroscopy (XPS) using surface etching by ionized argon. The spectra were recorded by an Escalab MK spectrometer (UK) using Mg K_α X-radiation (1253.6 eV, pass energy 20 eV). The samples were etched in the preparation chamber by ionized argon at a vacuum of 5×10^{-4} Pa. An accelerating voltage of ca. 15 kV and a beam current of 20 μA cm^{-2} were used. Etching was performed at a current of 20 μA, which corresponded to an etching rate of ca. 2 nm min^{-1}. Published data on binding energies (E_b) were used [30, 31, 32].

X-ray diffraction (XRD) investigations were carried out using Mo K_α radiation selected by a secondary graphite monochromator. The step-scan mode with a step $0.05°\times2\theta$ and a sampling time of 10 s/step in the range $10° \le 2\theta \le 40°$ was used.

The coated crystals were mounted in a special window of the corrosion cell, with the alloy side exposed to the cell compartment. The cell was made of Teflon with a corrosion chamber capacity of 80 mL. The cell was supplied with glass tubes for gas inlet and outlet and with a special window for the quartz specimen. The quartz was pressed onto the window via a Vitron O-ring. After the quartz mounting, a 20 mL portion of deoxygenated 5% NaCl solution was poured onto the bottom of the cell to maintain a wet atmosphere during measurements. The cell was hermetically closed by a Teflon cover and an argon stream was passed through the system in order to deoxygenate the cell. Then the argon flow rate was reduced to ca. 20 mL h^{-1} and the QCM measurements were started. The QCM experimental device was analogous to that described previously [29].

When a steady state of water adsorption had been achieved, a corrosion process was initiated by supplying oxygen gas with the same flow velocity as was set for argon. The relative humidity of the corrosive environment was not controlled, but it could be assumed to be near to 100%, because the corrosion chamber contained 5% NaCl solution and moisture take-up was negligible owing to the low gas flow velocity (20 mL h^{-1}). All experiments were carried out at the room temperature of 20 ± 2 °C.

For impedance studies of casting alloys as well as sputtered ones, a three-electrode, one-compartment cell made of glass was used. The casting alloy surface was polished by an abrasive SiC paper (grade 1000), rinsed with alcohol and water and then exposed for 24 h to air under ambient conditions. The specimen then was pressed via a Vitron O-ring onto a special window of the glass cell.

A saturated Ag/AgCl electrode was used as the reference electrode, and all potentials in this paper are referred to that electrode. A platinum foil served as a counter electrode. Impedance measurements were conducted by an IM6 apparatus (Zahner, Germany). The perturbation signal amplitude was 5 mV.

Table 1 Co-Cr-Mo compositions (in weight %) determined at 10 nm target depth and of the sputtered deposit on quartz. The sputtering chamber was pre-heated at 200 °C and under vacuum for 20 h. The samples were analysed by XPS after surface etching by ionized argon

Target (%)					
Co	Cr	Mo	Si	Mn	O
65	29	4.5	0.6	0.5	
Deposit (%)					
55	29	8.0	0.4	0.05	7.8

Table 2 Ni-Cr-Mo compositions (in weight %) determined at 10 nm target depth and of the sputtered deposit on quartz. The sputtering chamber was pre-heated at 200 °C and under vacuum for 20 h. The samples were analysed by XPS after surface etching by ionized argon

Target (%)					
Ni	Cr	Mo	Co	Be	O
72	13	11	1.8	1.8	
Deposit (%)					
68	15	7.0	1.0	1.8	6.0

Results and discussion

Results of XPS analysis of the MS coatings are presented in Tables 1 and 2. The data show that the content of any metal in the deposit is similar to that in the target. There is also ca. 6–8% of oxygen in the sputtered alloys. Such an amount of oxygen does not seem problematic for the QCM corrosion experiments, because the corroding samples are always partly oxidized.

The electrochemical impedance spectra, obtained under open circuit conditions for both sputtered and casting samples, are displayed in the form of Bode plots in Figs. 1 and 2. The corrosion resistance is usually reflected by the polarization resistance (R_p), which yields the low-frequency domain, in which impedance does not actually depend upon the frequency and the phase angle is near to 0°. However, owing to the high resistance of the alloys, such a domain could not be determined within a practical frequency range. The R_p value could be approximately estimated by a fitting procedure, when assuming an appropriate equivalent circuit. The experimental data in Figs. 1 and 2 (symbols) were well fitted (lines) assuming an equivalent circuit, which consisted of the solution resistance and R_p in parallel with a constant phase element (CPE) whose impedance is given by $Z_{CPE} = 1/C(j\Omega)^{-n}$. The CPE was used instead of the ideal capacity in order to take into account the capacitance of the space charge within a passive film (below it

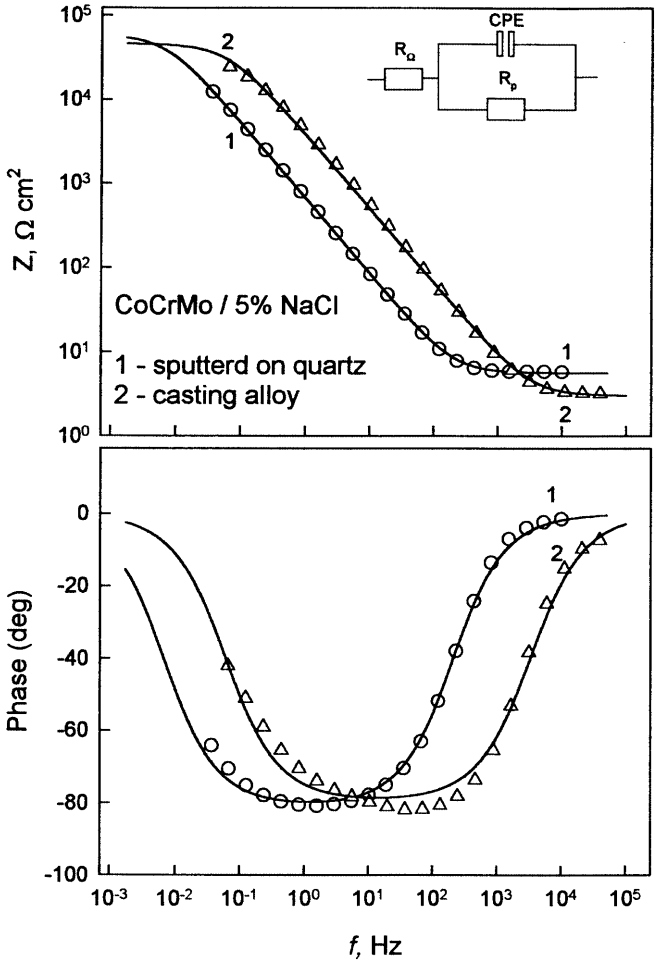

Fig. 1 Impedance diagram for magnetron-sputtered Co-Cr-Mo alloy (*1*) and casting alloy (*2*) in naturally aerated 5% NaCl solution at open circuit potentials (E_{ocp}): *1*, –0.09 $V_{Ag/AgCl}$; *2*, –0.17 $V_{Ag/AgCl}$. Measurements were started after 10-min immersion in the solution. The *symbols* represent experimental data and the *lines* are fitting results obtained by assuming the equivalent circuit, which consists of the solution resistance R_Ω and polarization resistance R_p in parallel with the constant phase element (CPE). Fitting parameters for the sputtered alloy (*curve 1*): $R_\Omega = 5.6\ \Omega\ cm^2$, $R_p = 59\ k\Omega\ cm^2$, $C = 116\ \mu F\ cm^{-2}$ ($n = 0.9$). Fitting parameters for the casting alloy (*curve 2*): $R_\Omega = 3.0\ \Omega\ cm^2$, $R_p = 47\ k\Omega\ cm^2$, $C = 18\ \mu F\ cm^{-2}$ ($n = 0.88$)

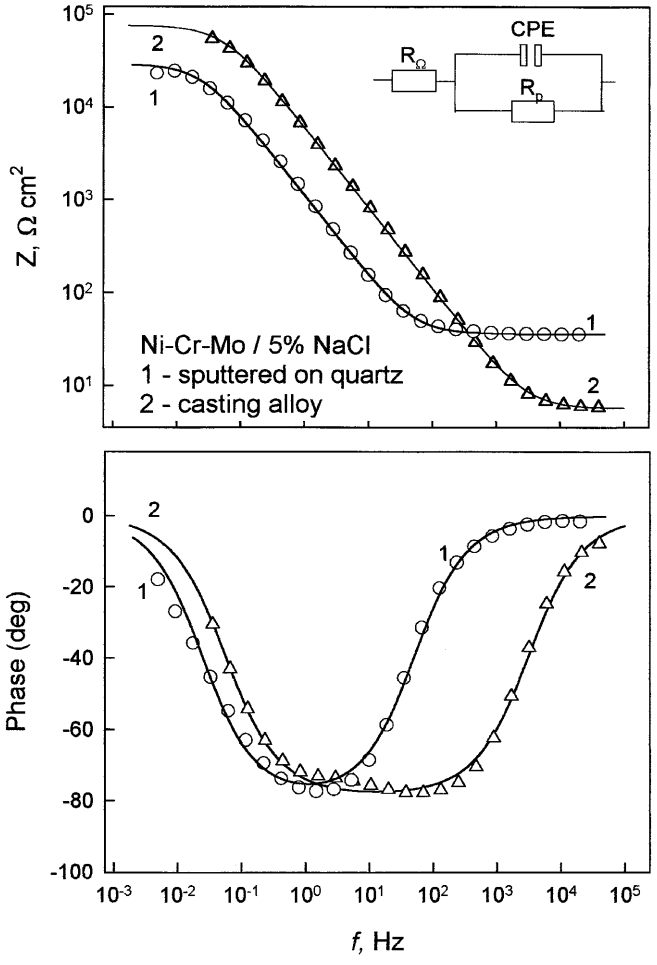

Fig. 2 Impedance diagram for magnetron-sputtered Ni-Cr-Mo alloy (*1*) and casting alloy (*2*) in naturally aerated 5% NaCl solution at open circuit potential potentials (E_{ocp}): *1*, –0.16 $V_{Ag/AgCl}$; *2*, –0.18 $V_{Ag/AgCl}$. Measurements were started after 10-min immersion in the solution. The *symbols* represent experimental data and the *lines* are fitting results obtained by assuming the equivalent circuit, which consists of the solution resistance R_Ω and the polarization resistance R_p in parallel with the constant phase element (CPE). Fitting parameters for the sputtered alloy (*curve 1*): $R_\Omega = 36\ \Omega\ cm^2$, $R_p = 29.3\ k\Omega\ cm^2$, $C = 62\ \mu F\ cm^{-2}$ ($n = 0.88$). Fitting parameters for the casting alloy (*curve 2*): $R_\Omega = 5.6\ \Omega\ cm^2$, $R_p = 76\ k\Omega\ cm^2$, $C = 11\ \mu F\ cm^{-2}$ ($n = 0.9$)

will be shown that the passive film on both Co-Cr-Mo and Ni-Cr-Mo alloys is composed mainly of Cr_2O_3).

The polarization resistance of sputtered Co-Cr-Mo alloy (Fig. 1) did not differ greatly from the resistance of the casting alloy ($R_p = 59$ kΩ cm^2 and $R_p = 47$ kΩ cm^2, respectively). The double layer capacities, however, differed considerably ($C_s = 116$ μF cm^{-2} for the sputtered surface on quartz and $C_c = 18$ μF cm^{-2} for the mechanically polished alloy). The condition $C_s > > C_c$ is typical of sputtered on quartz and mechanically polished specimens, which is mainly due to a greater actual area of the quartz substrate (Fig. 3). Obviously, the mechanically polished surface is smoother than that on quartz. An even smoother coating is observed on glass.

In order to compare the corrosion resistance of both specimens, it is necessary to relate the R_p values to the same actual area. An approximate correction could be done by assuming the ratio C_s/C_c as a criterion for the difference in the actual surface areas. To be precise, such a correction is only true when the relative permittivity and the thickness of the oxide layers on both specimens differ negligibly. As will be discussed below, the surface layers on Co-Cr-Mo as well as on Ni-Cr-Mo are composed predominantly of Cr_2O_3. The XPS analysis performed using surface etching by ionized argon showed that the thickness of the oxide layers developed in NaCl solution does not differ considerably for both the sputtered and polished specimens (Sudavičius A, Samulevičienė M, Leinartas K, unpublished data). Therefore, the significant difference in the double layer capacities ($C_s = 116$ μF cm^{-2} and $C_c = 18$ μF cm^{-2}) may be attributed mainly to different actual surface areas of the sputtered and mechanically polished specimens (Fig. 3).

The corrected polarization resistance for the sputtered alloy was $R_p' = (C_s/C_c) \times R_p = 377$ kΩ cm^2. The latter value is significantly higher than that for the casting alloy ($R_p = 47$ kΩ cm^2; Fig. 1). We can conclude, therefore, that the corrosion resistance of the sputtered deposit is higher than the resistance of the casting alloy.

Acting in the above-described manner, we obtained for the sputtered Ni-Cr-Mo alloy a corrected polarization resistance of $R_p' = (C_s/C_c) \times R_p = 165$ kΩ cm^2, while the resistance of the cast alloy was $R_p = 76$ kΩ cm^2. Once again, it can be concluded that the sputtered alloy had a superior corrosion resistance.

The XRD pattern of the sputtered Ni-Cr-Mo alloy differed considerably from that of the casting alloy (Fig. 4). Sharp XRD peaks of the latter (pattern a) indicate a perfect crystalline structure, which consisted

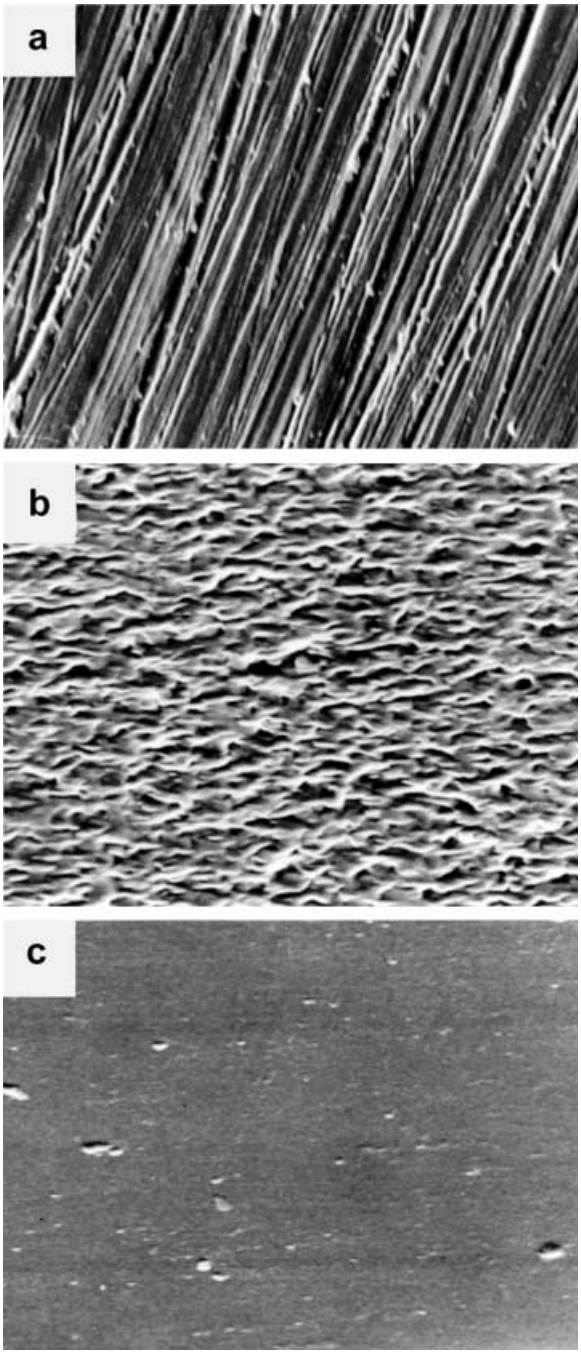

Fig. 3 SEM micrographs (×1000) of the mechanically polished Co-Cr-Mo surface (**a**) and of those sputtered on quartz (**b**) as well as on glass (**c**) substrates

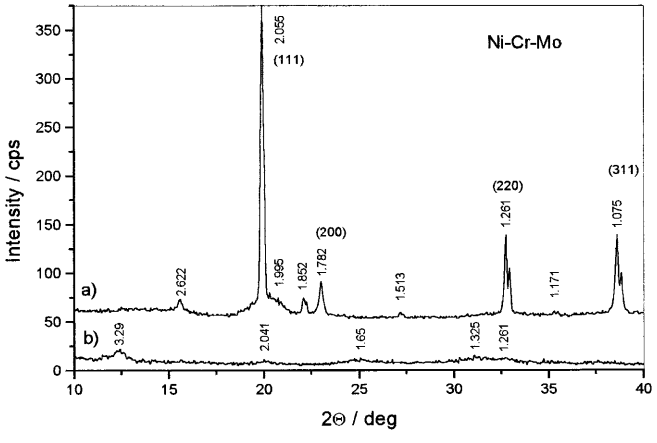

Fig. 4 XRD patterns for casting Ni-Cr-Mo alloy (a) and magnetron sputtered alloy (b) on quartz; MoK_α radiation

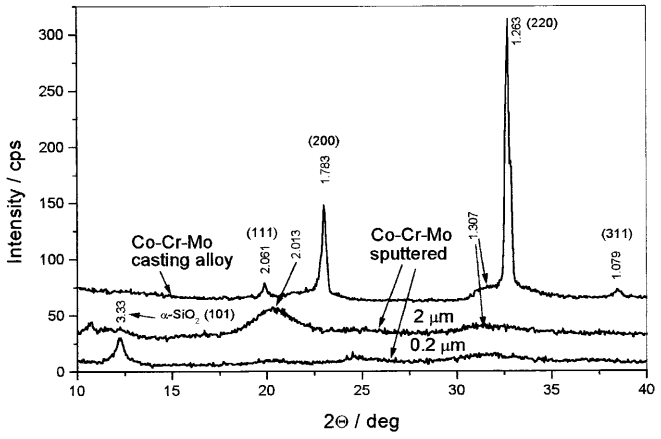

Fig. 5 XRD patterns for casting Co-Cr-Mo alloy and magnetron-sputtered alloy (0.2 μm and 2 μm thick) on quartz; Mo K_α radiation

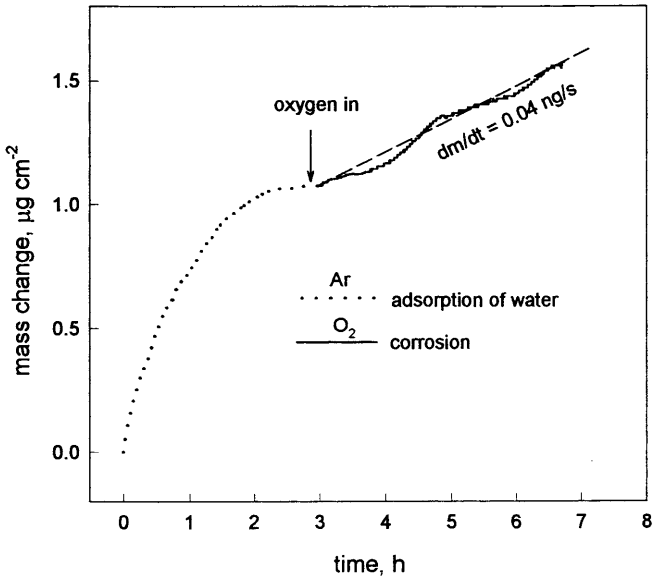

Fig. 6 Ni-Cr-Mo mass change determined by QCM in a wet argon atmosphere (*dotted line*) and during corrosion (*full trace*), which was initiated by supplying oxygen gas. The oxygen flow rate was 20 mL h^{-1}

of at least two phases. Peaks of one phase are indexed and it may be a substitution alloy of molybdenum in nickel. There were no sharp peaks in the pattern of the sputtered alloy, which implied an amorphous structure of the deposit. Analogously, Fig. 5 reveals a crystalline structure for the casting Co-Cr-Mo alloy and an amorphous structure for the sputtered films (both 0.2 μm and 2 μm thickness).

Figure 6 shows a mass versus time plot obtained for Ni-Cr-Mo in argon and oxygen atmospheres. The mass increase in argon represents the dynamics of water adsorption on the alloy surface. The moisture layer reached a maximum thickness after ca. 2.5 h and the mass of the layer was $\Delta m \approx 1.1$ μg cm^{-2}. This value is in good agreement with an analogous value determined by Lee and Staehle [33] on gold at 25 °C and 100% relative humidity. The authors assumed that the actual monolayer capacity of water on gold was 3.1033×10^{-8} g cm^{-2} multiplied by the surface roughness (the ratio between the actual and planar surface areas, which was estimated by a factor of 2 for the evaporated gold surface).

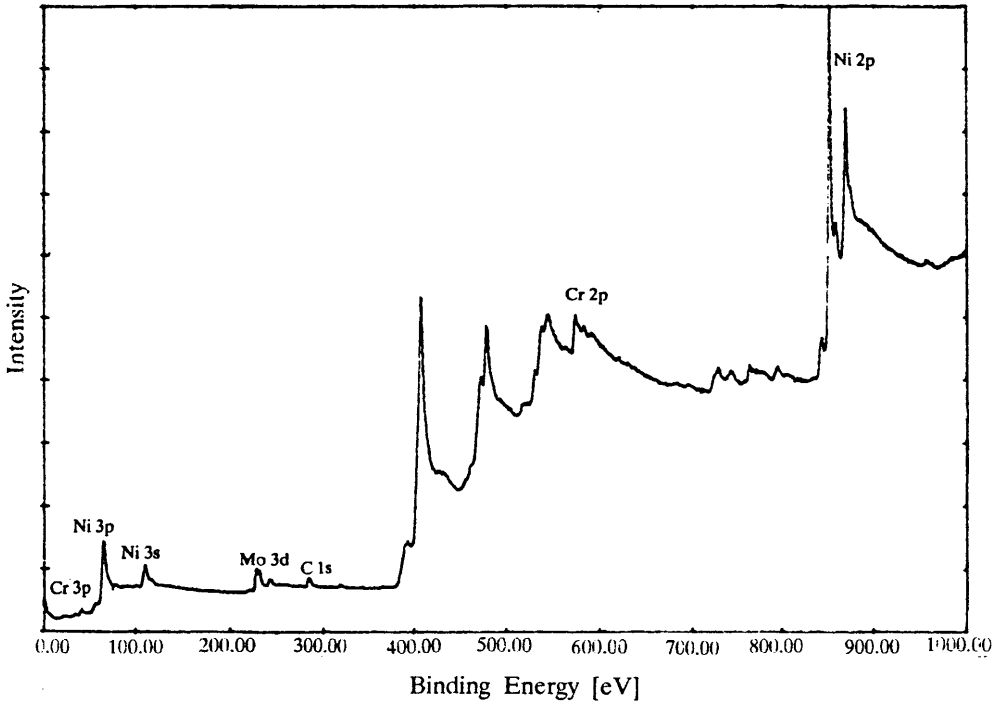

Fig. 7 A survey XPS spectrum recorded for Ni-Cr-Mo sputtered alloy after the experiment described in Fig. 6

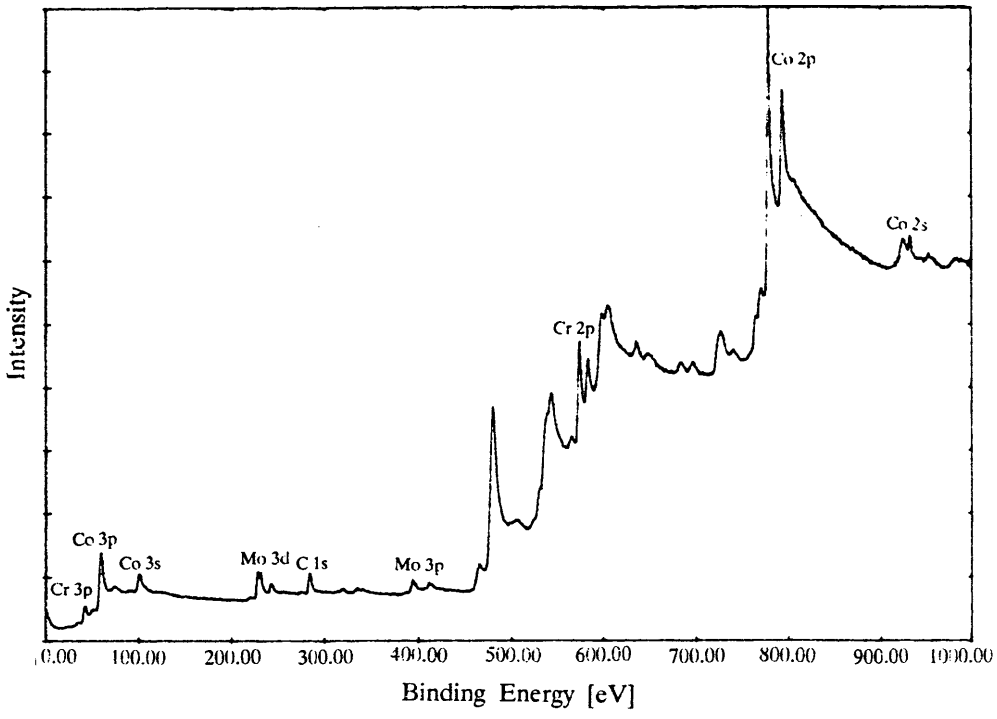

Fig. 8 A survey XPS spectrum recorded for Co-Cr-Mo sputtered alloy after the experiment described in Fig. 6

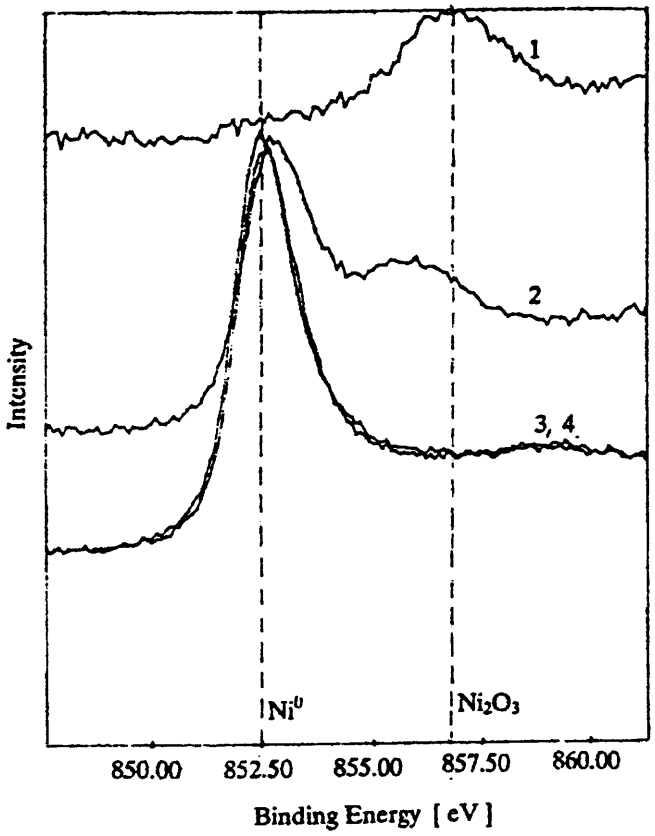

Fig. 9 XPS spectra (Ni $2p_{3/2}$) recorded for Ni-Cr-Mo after the experiment described in Fig. 6. Surface sputtering time by ionized argon (in s): *1*, 0; *2*, 30; *3*, 90; *4*, 120

After a steady state of water adsorption had been achieved, a corrosion process was initiated by introducing oxygen gas (Fig. 6). Following some induction time, the microbalance indicated an increase in the sample mass, which was due to oxygen bonding by the corroding surface. The average rate of mass gain in Fig. 6 is $dm/dt = 0.04$ ng s^{-1}. The mass gain rate at any time could be estimated from a corresponding dm/dt slope of the mass curve.

The corrosion rate could also be expressed in electric units (A cm^{-2}), which is a common practice in corrosion investigations by electrochemical methods. The ratio between the oscillation frequency change of the quartz resonator and the mass change is given by [27, 34, 35]:

$$j_{corr} = -(nFC/\Delta M)(df/dt) \quad (1)$$

where j_{corr} is the corrosion current density (A cm^{-2}), df/dt is the rate of change of the quartz oscillation frequency, F is the Faraday constant, n is the number of electrons in the corrosion reaction, ΔM is the molar mass of the group responsible for the mass gain during corrosion (O, OH, OOH, etc.), and C is the proportional coefficient between the frequency and the mass change. According to Sauerbrey's equation [36], $C = 18$ ng Hz^{-1} cm^{-2} when the main resonance frequency is $f_0 = 5$ MHz.

Assuming the mass change rate $dm/dt = 1$ ng s^{-1} and the above C value, we can simplify the ratio of Eq. 1 to:

$$j_{corr} = 9.65 \times 10^{-5}(n/\Delta M) \quad (2)$$

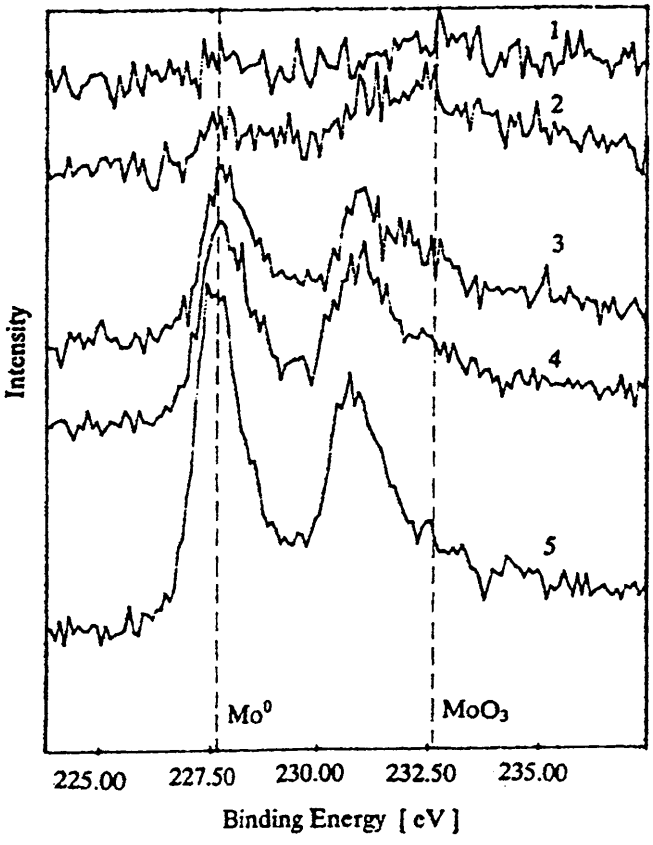

Fig. 10 XPS spectra (Mo $3d_{5/2}$) recorded for Ni-Cr-Mo after the experiment described in Fig. 6. Surface sputtering time by ionized argon (in s): *1*, 0: *2*, 30; *3*, 90; *4*, 120; *5*, 360

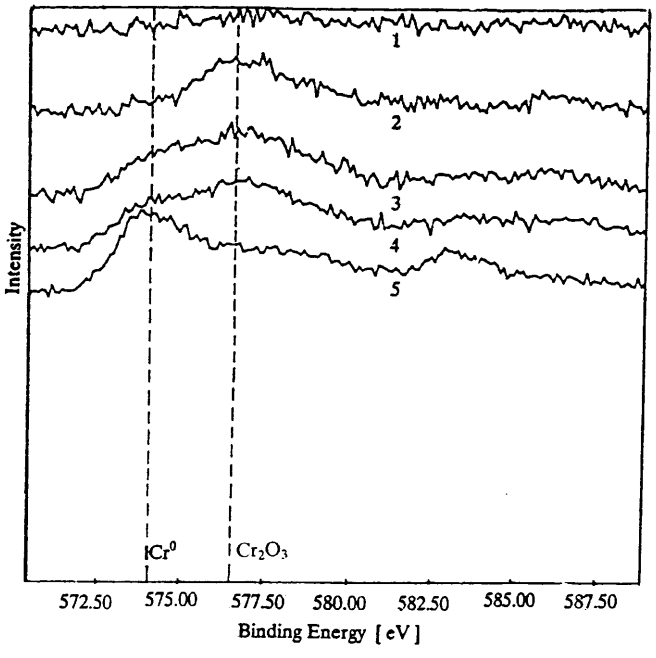

Fig. 11 XPS spectra (Cr $2p_{3/2}$) recorded for Ni-Cr-Mo after the experiment described in Fig. 6. Surface sputtering time by ionized argon (in s): *1*, 0; *2*, 30; *3*, 90; *4*, 120; *5*, 360

The j_{corr} calculations according to Eq. 2 for different oxides (M_2O, MO, M_2O_3 MO_2 and MO_3) give the same value of $j_{corr} = 12$ μA cm^{-2} (because of the same ratio $n/\Delta M$). Thus, the calculation of j_{corr} does not require knowledge of what oxides and in which proportion they form during corrosion; it is enough to know that the corrosion products are oxides.

The sample was analysed by XPS after corrosion in oxygen (Figs. 7, 8, 9, 10, 11). It appeared that all components were in an oxidized state on the surface, viz. Ni_2O_3 ($E_b = 856.7$ eV; Fig. 9), MoO_3 ($E_b = 232.6$ eV; Fig. 10) and Cr_2O_3 ($E_b = 576.6$ eV; Fig. 11). However, in deeper levels, only Cr_2O_3 was predominant, as was evident from the spectra recorded after 90 min of surface sputtering by ionized argon. Assuming the oxides as corrosion products, we could estimate according to Eq. 1 an average corrosion current density for Ni-Cr-Mo to be as high as $j_{corr} = 0.48$ μA cm^{-2} (Fig. 6).

Figure 12 gives data on Co-Cr-Mo corrosion in an oxygen-containing atmosphere. Surface analysis by XPS showed that, analogously to the Ni-Cr-Mo alloy, Cr_2O_3 prevailed on the corroded Co-Cr-Mo specimen (spectra not shown). The average mass change value of $dm/dt = 0.08$ ng s^{-1} yielded, according to Eq. 1, $j_{corr} = 0.96$ μA cm^{-2}. This corrosion rate is twice as high as the value calculated above for the Ni-Cr-Mo alloy.

Figure 13 represents the QCM data on alloy corrosion in NaCl solution open to the air. The distinctive mass growth after electrode immersion ($dm/dt \approx 1$ ng s^{-1}) implies corrosion with accumulation of barely soluble corrosion products on the surface. The mass increase of Ni-Cr-Mo stopped after ca. 25-min immersion and then a slight mass decrease was observed ($dm/dt \approx -0.05$ ng s^{-1}). Thus, the protective surface layer reached its maximum thickness, the mass of which is ca.

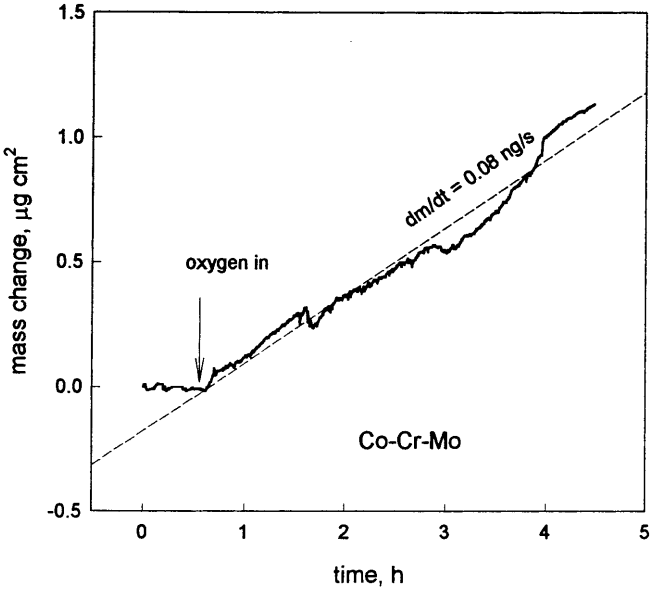

Fig. 12 Co-Cr-Mo mass change determined by QCM during corrosion, which was initiated by supplying oxygen gas (indicated by an *arrow*). The oxygen flow rate was 20 mL h^{-1}

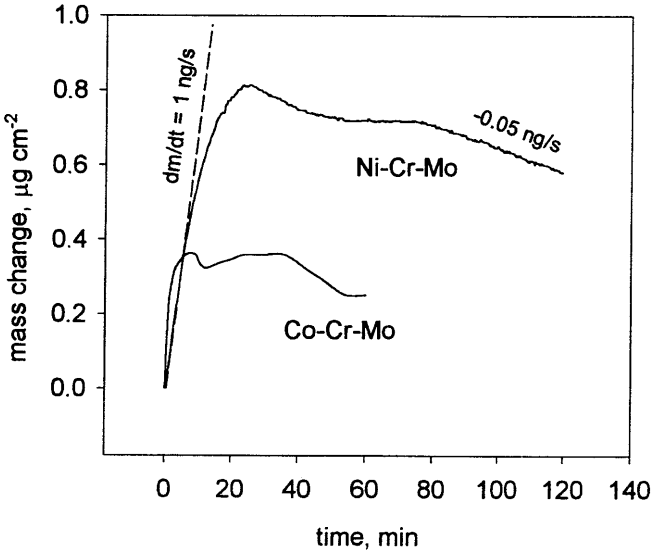

Fig. 13 Ni-Cr-Mo and Co-Cr-Mo mass change during immersion in 5% NaCl open to the air determined by QCM

0.8 μg cm^{-2}, and afterwards transfer of metal ions to the solution dominated. The mass of an analogous layer on Co-Cr-Mo was about 0.35 μg cm^{-2}.

The XPS investigations showed that the oxygen-containing layer developed on Co-Cr-Mo and on Ni-Cr-Mo in NaCl solution was composed predominantly of Cr_2O_3 [37]. Assuming this, we can obtain from the initial slope of 1 ng s^{-1} in Fig. 11 according to Eq. 1 the value of $j_{corr} = 12$ μA cm^{-2}. This is a rather high corrosion current, which indicates an active surface state in the initial corrosion stages. (It should be noted that, according to QCM data, the diffusion-limited current for oxygen reduction on an active cadmium electrode in a naturally aerated solution is about 50 μA cm^{-2} [27].)

For corrosion current calculations it is important to know which part of the ionized metal is converted to sparingly soluble compounds and remains on the corroding surface, and what is transferred into the solution phase. Thus, corrosion resistance evaluation in solutions seems to be more complicated than in gaseous environments, where corrosion products remain on the surface. It should also be noted that, under certain conditions, in solutions a complete accumulation of corrosion products on the surface could be ensured, as has been demonstrated when studying Au-Pd-In alloy in simulated physiological solutions [16].

Conclusions

Magnetron-sputtered Ni-Cr-Mo and Co-Cr-Mo alloys on quartz had an amorphous structure with a decreased corrosion activity when compared to conventional crystalline alloys. The alloy sputtering therefore is of increasing interest as a tool to produce highly corrosion-resistant coatings.

Quartz crystal nanogravimetry appeared to be an effective approach for corrosive characterization of sputtered alloys in gaseous environments. The advantages include information continuity, nanogram resolution and the possibility to combine the QCM measurements with other methods (for instance, spectroscopy).

In principle, the microgravimetric corrosion testing is also applicable to liquids; however, the estimation of corrosion rates in liquids could be more complicated by corrosion product transfer to the solution phase.

References

1. Mehmood M, Akiyama E, Habazaki H, Kawashima A, Asami K, Hashimoto K (1999) Corros Sci 41:1871
2. Mehmood M, Akiyama E, Habazaki H, Kawashima A, Asami K, Hashimoto K (1998) Corros Sci 40:1
3. Mehmood M, Akiyama E, Habazaki H, Kawashima A, Asami K, Hashimoto K (1999) Corros Sci 41:477
4. Li X-Y, Akiyama E, Habazaki H, Kawashima A, Asami K, Hashimoto K (1999) Corros Sci 41:1849
5. Park P-Y, Akiyama E, Habazaki H, Asami K, Hashimoto K (1995) Corros Sci 37:1843
6. Frankel GS, Newman RC, Jahnes CV, Russak MA (1993) J Electrochem Soc 140:2192
7. Habazaki H, Shimizu K, Skeldon P, Thompson GE, Wood GC (1997) Thin Solid Films 300:131
8. Habazaki H, Takahiro K, Yamaguchi S, Shimizu K, Skeldon P, Thompson GE, Wood GC (1999) J Electrochem Soc 146:2502
9. Ryan MP, Laycock NJ, Isaacs HS, Newman RC (1999) J Electrochem Soc 146:91
10. Liu ZY, Gao W, Dahm KL, Wang FH (1998) Acta Mater 46:1691
11. Landolt D, Robyr C, Mettraux P (1998) Corrosion 54:772
12. Schmutz P, Landolt D (1999) Corros Sci 41:2143
13. Oliveira JC, Cavaleiro A, Brett CMA (2000) Corros Sci 42:1881
14. Li X-Y, Akiyama E, Habazaki H, Kawashima A, Asami K, Hashimoto K (1996) Corros Sci 38:1269
15. Juzeliūnas E, Leinartas K, Samulevičienė M, Jelinskienė D, Sudavičius A, Miečinskas P, Lisauskas V, Vengalis B (2000) In: Hui D (ed) Proceedings of the 7th annual international conference on composites engineering, Denver, Colorado, USA, p 405
16. Leinartas K, Miečinskas P, Sudavičius A, Jelinskienė D, Juškėnas R, Lisauskas V, Vengalis B, Juzeliūnas E (2001) J Appl Electrochem (in press)
17. Leinartas K, Samulevičienė M, Bagdonas A, Sudavičius A, Lisauskas V, Juzeliūnas E (2001) Electrochem Commun 3:473
18. Hashimoto K, Osaka K, Matsumoto T, Shimodara S (1976) Corros Sci 16:71
19. Rice DW, Phipps PBP, Tremourex R (1979) J Electrochem Soc 126:1459
20. Zakipuor S, Leygraf C, Portnoff G (1986) J Electrochem Soc 133:873
21. Deakin MR, Melroy O (1989) J Electrochem Soc 136:349
22. Schumacher R, Mueller A, Stoeckel W (1987) J Electroanal Chem 216:127
23. Forslund M, Leygraf C (1996) J Electrochem Soc 143:839
24. Forslund M, Majoros J, Leygraf C (1997) J Electrochem Soc 144:2637
25. Aastrup T, Leygraf C (1997) J Electrochem Soc 144:2986
26. Stratmann M, Fürbeth W, Grundmeier G, Lösch R, Reinartz C (1995) In: Marcus P, Oudar J (eds) Corrosion mechanisms in theory and practice. Dekker, New York, p 373

27. Juzeliūnas E (1992) Elektrokhimiya 28:1656
28. Juzeliūnas E, Samulevičienė M (1992) Electrochim Acta 37:2611
29. Juzeliūnas E, Kalinauskas P, Miečinskas P (1996) J Electrochem Soc 143:1525
30. Wagner CD, Riggs WM, Davis LE, Moulder JF, Muilenberg GE (1978) Handbook of X-ray photoelectron spectroscopy, Perkin Elmer, Minn
31. Briggs D (ed) (1983) Practical surface analysis by Auger and X-ray photoelectron spectroscopy. Wiley, New York
32. Cimino A, De Angelio BA, Lucketti A, Minelli G (1976) J Catal 45:316
33. Lee S, Staehle RW (1996) Corrosion 52:843
34. Leng A (1991) Diploma thesis, University of Düsseldorf
35. Stratmann M, Fürbeth W, Grundmeier G, Lösch R, Reinartz CR (1995) In: Markus P, Oudar J (eds) Corrosion mechanisms in theory and practice. Dekker, New York, p 401
36. Sauerbrey G (1959) Z Phys 155:206
37. Samulevičienė M, Linčiūtė R, Sližys R, Sudavičius A, Juzeliūnas E (1998) Chemija 2:109